Decoupling the shape parameter to assess gold nanorod uptake by mammalian cells†

C. Kinnear,‡[a] L. Rodriguez-Lorenzo,[a] M. J. D. Clift,§[a] B. Goris,[b] S. Bals,[b] B. Rothen-Rutishauser[a] and A. Petri-Fink*[a,c]

The impact of nanoparticles (NPs) upon biological systems can be fundamentally associated with their physicochemical parameters. A further often-stated tenet is the importance of NP shape on rates of endocytosis. However, given the convoluted parameters concerning the NP–cell interaction, it is experimentally challenging to attribute any findings to shape alone. Herein we demonstrate that shape, below a certain limit, which is specific to nanomedicine, is not important for the endocytosis of spherocylinders by either epithelial or macrophage cells *in vitro*. Through a systematic approach, we reshaped a single batch of gold nanorods into different aspect ratios resulting in near-spheres and studied their cytotoxicity, (pro-)inflammatory status, and endocytosis/exocytosis. It was found that on a length scale of ~10–90 nm and at aspect ratios less than 5, NP shape has little impact upon their entry into either macrophages or epithelial cells. Conversely, nanorods with an aspect ratio above 5 were preferentially endocytosed by epithelial cells, whereas there was a lack of shape dependent uptake following exposure to macrophages *in vitro*. These findings have implications both in the understanding of nanoparticle reshaping mechanisms, as well as in the future rational design of nanomaterials for biomedical applications.

Introduction

A thorough material characterization is crucial in order to unambiguously attribute any biological interaction to a specific nanoparticle (NP) physico-chemical property.[1,2] Of the most widely studied shapes, spherocylinders, cylinders and ellipsoids are normally categorized by one characteristic: aspect ratio.[3–6] This physical parameter of non-isotropic engineered nanomaterials is highly desirable, especially within proposed applications for nanomedicine (*e.g.* cell-based specific therapeutics).[7] In this context, we asked the question "how does aspect ratio affect cellular uptake?". Many non-trivial and complex answers can be given as shown by often contradictory results, originating from entangled dependent and independent experimental variables, published for a plethora of different anisotropic nanomaterials.[4,6,8,9] It is important to highlight that this study does not address the extreme case of highly anisotropic fibers, such as asbestos or carbon nanotubes with lengths on the micron scale, which are well-known to have a shape-dependent, biological impact.[10,11]

One of the earliest studies was by Chithrani *et al.* on cetyltrimethylammonium bromide (CTAB) coated gold nanorods where a negative correlation between aspect ratio and cellular uptake was found.[12,13] However, recent research has highlighted the significance of multiple convoluted variables such as ligand cytotoxicity,[14] particokinetics,[15,16] colloidal stability[17] and nanoparticle volume,[18] among others. An appropriate example of this is the study of Qiu *et al.* who found a similar result as Chithrani *et al.* except that upon passivating the surface with polyelectrolytes the apparent shape-dependent uptake was diminished.[6]

Thus, to decipher the challenge posed above it is necessary to engineer and control the aspect ratio above all the other physicochemical characteristics of anisotropic nanomaterials (*e.g.* gold nanorods). This is highly pertinent, as changing the morphology in this regard requires a separate synthesis with a corresponding different chemical environment. Therefore, maintaining consistency in key parameters, such as NP volume, width or ligand density, from batch to batch is (nearly) impossible. The problem is compounded further by the dominant role that surface chemistry plays in mediating the rate of cellular uptake.[6]

Therefore, in order to maintain consistency, we describe the use of one 'master' batch of high aspect ratio gold nanorods

[a]*Adolphe Merkle Institute, University of Fribourg, Fribourg 1700, Switzerland*
[b]*Electron Microscopy for Materials Research (EMAT), University of Antwerp, Antwerp 2020, Belgium*
[c]*Chemistry Department, University of Fribourg, Fribourg 1700, Switzerland. E-mail: alke.fink@unifr.ch*

†Electronic supplementary information (ESI) available: Additional figures and tables. See DOI: 10.1039/c6nr03543d

‡Present address: School of Chemistry and Bio21 Institute, University of Melbourne, Victoria, Australia.
§Present address: In Vitro Toxicology Group, Swansea University Medical School. Singleton Park Campus, Swansea, SA2 8PP, Wales, UK.

(GNRs, 113 × 16 nm) to generate lower aspect ratio NPs through a thermal reshaping mechanism. The resulting chemical surface, morphology, and colloidal stability are extensively characterized with a view to compare near-identical NPs which differ only in one variable, 'shape'. Specifically, all GNRs had near-identical NMR spectra; volume and surface area distributions; zeta-potentials; hydrodynamic parameters from depolarized dynamic light scattering (DDLS); and diffusion and sedimentation coefficients and exhibited complete colloidal stability in supplemented cell culture media over 24 h. Despite these similarities, a two-fold increase in intracellular gold was found for GNRs of an aspect ratio of 7.2 compared with 4.8 or less in the two epithelial cell types tested. Additionally, all GNRs were neither cytotoxic nor (pro-)inflammogenic as assessed by the quantity of extracellular lactate dehydrogenase (LDH) and (pro-)inflammatory cytokines/chemokines (tumor necrosis factor (TNF)-α and interleukin (IL)-8) respectively. These data are important to understand the behavior of non-isotropic nanomaterials towards their potential application within theranostic applications *in vivo*. Additionally, they suggest that in order to benefit from the physical properties of anisotropic nanomaterials, their aspect ratio should be above a certain threshold. This is particularly relevant given the advantage shape imparts upon bacteria and viruses,[19] as well as the recent examples of GNR promoted migration of metastatic breast cancer cells *in vitro*,[20] or the targeting of lung and brain epithelium with anisotropic NPs.[21]

Results and discussion

Synthesis and detailed characterization of nanorods of varied aspect ratio

A single batch of high aspect ratio GNRs was synthesized *via* a modified seed mediated method, using a binary surfactant system of CTAB and sodium oleate (NaOL), followed by functionalization with polyvinylpyrrolidone (PVP) and transfer to dimethylformamide (DMF).[22,23] Upon heating to 140 °C, the aspect ratio of the GNRs decreased through surface melting at the tips and deposition on the sides.[24] This process can be finely tuned through the ratio of polymer to surfactant; excess PVP arrests the reshaping while excess CTAB dissolves the GNRs (Fig. S1 and S2†). Through halting the reshaping at different times, over 6 h, four dispersions of GNRs were obtained with varying aspect ratios as evident by their localized surface plasmon resonance (LSPR, Fig. 1): GNR-7.2 (113 × 16 nm, aspect ratio 7.2), GNR-4.8 (84 × 18 nm, aspect ratio 4.8), GNR-2.6 (62 × 24 nm, aspect ratio 2.6), and GNR-1.9 (55 × 29 nm, aspect ratio 1.9). The reshaped GNRs were essentially equivalent in terms of relative quantities of surface adsorbed ligands, as measured by ^{1}H-NMR (Fig. 1b, S3–5 and Table S1†). Additionally, their zeta-potential and hydrodynamic sizes were shown to be similar using DDLS, although this is not surprising considering that the GNRs are from the same batch (Table S2†). To enable a comparison of hydrodynamic diameters across orthogonal techniques, a spherical model was used for both NTA and DDLS analysis although a spherocylindrical model can also be applied.[25]

Impact of thermal reshaping on nanorod crystallinity

In order to undergo a shape change, there needs to be a corresponding alteration in crystal structure, at least in terms of relative areas of surface facets. To assess this, nanorods before and after reshaping were characterized using high-angle annular dark-field scanning transmission electron microscopy (HAADF-STEM) tomography. Fig. 2a–c present HAADF-STEM projection images of GNRs before and after thermal reshaping for 1.5 h and 6 h respectively. The corresponding tomography

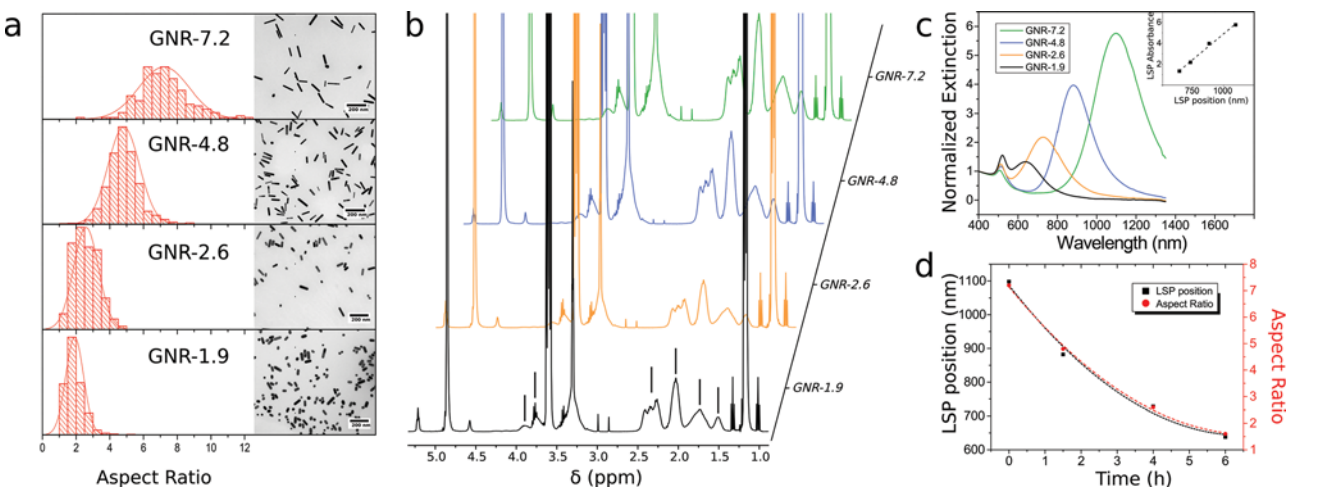

Fig. 1 Reshaping of gold nanorods. (a) Aspect ratio, by TEM, of the four reshaped GNR samples. Inset: representative TEM micrographs. (b) ^{1}H NMR of reshaped GNRs where the lines indicate the adsorbed polymer. All other peaks were identified as solvent resonances or residual reagents (ESI†). (c) Vis-NIR spectra of reshaped GNRs. Inset: linear correlation between the position of the longitudinal surface plasmon resonance and the intensity of the absorption. (d) Effect of the reshaping time on the position of the longitudinal surface plasmon resonance and aspect ratio. Dashed lines are quadratic fits as a guide to the eye.

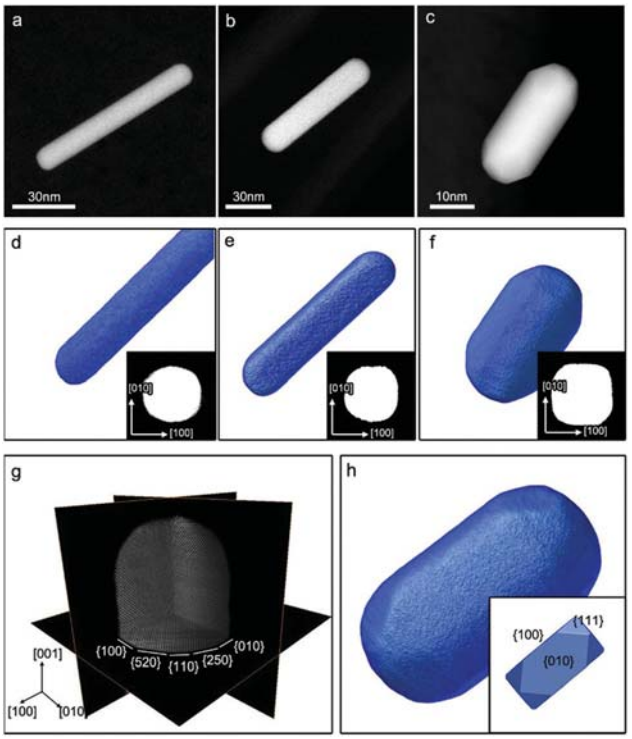

Fig. 2 3D structure of gold nanorods before and after thermal reshaping. (a–c) HAADF-STEM projection images for the GNRs before (a) and after 1.5 h (b) and 6 h (c) of thermal annealing. (d–f) The corresponding tomographic reconstructions showing a transformation from a rounded nanorod of high aspect ratio towards nanorods with a lower aspect ratio and a squarer cross section. (g) Tomography reconstruction showing the atomic lattice of the initial GNRs and a combination of {520} and {100} side facets. (h) Characterization of the GNR surface facets after 6 h of reshaping, presenting {100} and {010} facets with truncated {111} tips.

reconstructions show a transformation from a rounded nanorod of high aspect ratio to a lower aspect ratio nanorod with an increased squared cross section (Fig. 2d–f). However, in order to unambiguously determine the surface facets of the GNRs prior to thermal annealing, a reconstruction with a resolution up to the atomic scale is required (Fig. 2g). This reconstruction reveals an octahedral, near-spherical, cross-section composed of {100}, {520}, and potentially {110} facets, deviating from the traditional combination of {010} and {110} facets for GNRs synthesized with CTAB as the sole surfactant.[26] The deviation is remarkably similar to the structure observed when a gemini surfactant is used during the synthesis, indicating the use of NaOL has a fundamental impact on the growth kinetics and surface energy of higher index facets in order to render them energetically favorable.[26] After 6 h of thermal treatment the cross section becomes progressively more square-like and the truncation at the {111} facets of the tip of the nanorod becomes more pronounced, as observed in the 3D visualization (Fig. 2h). Interestingly, the sides are composed primarily of {100} facets indicating that the atoms at the tip likely redeposit on the higher-energy {520} and {250} planes, which is in line with other studies that reduced gold salt onto preformed GNR seeds.[27,28] Additionally, the observed growth direction was along the [001] zone axis with a persistent bulk face-centered cubic structure throughout.

The mean volume, estimated from low resolution transmission electron microscopy (TEM) as described in the ESI,† of each shape was similar indicating the reshaping mechanism is primarily dissolution and re-deposition triggered by CTAB and PVP, as opposed to Ostwald ripening (Table S3†). Furthermore, the number concentration after reshaping *via* nanoparticle tracking analysis (NTA) was similar across the different shapes (Table S3†). Taking this into consideration with the above results, it can be concluded that the reshaped GNRs differ solely in terms of shape as opposed to surface chemistry or volume.

Colloidal stability

Cellular uptake of NPs depends on the delivered cellular dose, which is a function of the NP diffusion and sedimentation coefficients – both of which are similar between the different batches of reshaped GNRs.[15] Colloidal stability though can greatly alter these parameters. Therefore, the stability of the four shapes in supplemented cell culture media containing 10% fetal bovine serum (FBS) was probed by DDLS, NTA and Vis-NIR spectroscopy. Any aggregation would result in a large shift and broadening of their LSPR, which was not observed for any of the four samples (Fig. 3a) after 24 h at 37 °C and 5% CO_2. Nevertheless, a small red-shift was found and can be associated with the evolution of the soft protein corona with time.[29] This is supported by NTA with a slight increase in the hydrodynamic diameter after 24 h (Fig. 3b). If the reason for the increase in size, and the red-shift of the LSPR, was aggregation then fewer NPs would be counted by NTA (aggregates are only counted as a single particle). The fact that this does not occur proves that the GNRs are colloidally stable over the exposure period.

Shape-dependent endocytosis of gold nanorods

The uptake of GNRs was investigated *via* a 4 h or 24 h exposure to the two epithelial cell lines (A549 and HeLa), and a macrophage cell line (J774A.1) by inductively coupled plasma optical emission spectroscopy (ICP-OES) after an iodine etch to remove membrane bound GNRs,[30] dark-field light microscopy, and TEM. Such a combination of methods is important to understand the interaction of GNRs at the single cell level since each of the techniques has both advantages and limitations.[31] Given the small depth of field for darkfield light microscopy, and select TEM images, it can be observed that all three cell types internalize the nanorod samples. Additionally, iodine rapidly etches all extracellular gold therefore the term uptake is used hereafter in lieu of cell associated. Each cell type was used in order to represent typical cell types that may be exposed to nanomaterials *via* inhalation therapy (*i.e.* the lung) or direct injection into the bloodstream. Furthermore, they allow for a fundamental read-across with other ongoing research in the field of NP-cell interactions.[9] Across both time points, the macrophages internalised the same number of

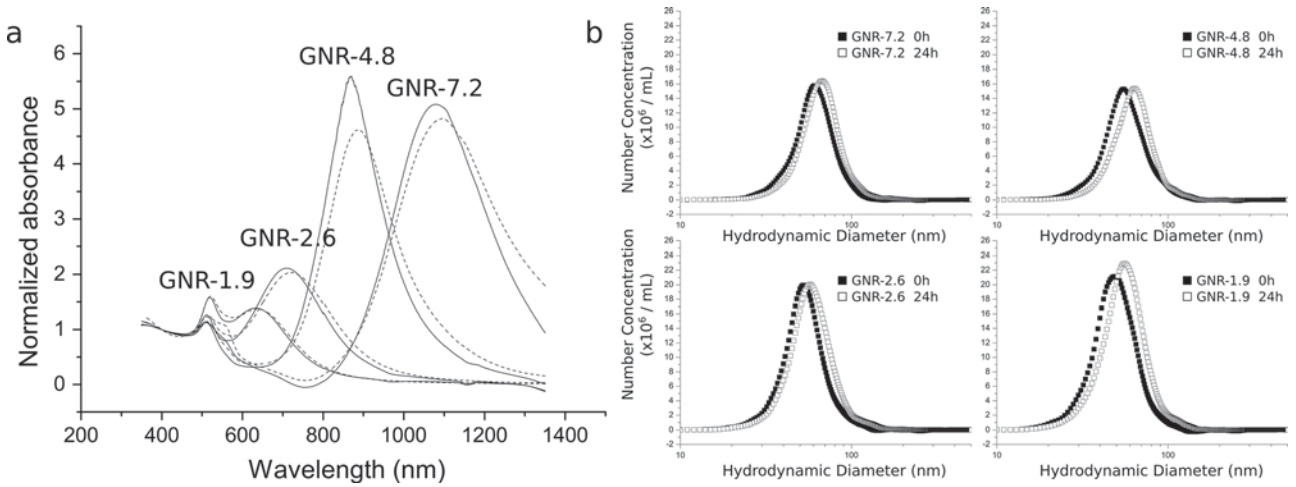

Fig. 3 Colloidal stability. (a) Vis-NIR spectra of reshaped GNRs before and after (dashed line) 24 h incubation in supplemented RPMI at 37 °C and 5% CO_2. (b) Hydrodynamic diameter by NTA after 24 h in supplemented RPMI.

GNRs per cell irrespective of their aspect ratio (Fig. 4). In contrast to this, higher levels of intracellular gold were found for both epithelial cell lines exposed to the longest GNRs, while no differences were observed for aspect ratios of 4.8 or below. These trends persist within each cell type when the data is expressed either as total intracellular gold or the number of NPs per seeded cell, as expected due to the similar volumes of the four GNRs (Fig. S6†).

The greater uptake for longer GNRs was qualitatively confirmed by dark-field light microscopy of HeLa cells; cells exposed to GNR-7.2 possessed more intracellular particles with intense scatter than GNR-4.8 at both 4 h and 24 h (Fig. 5e and f).[32] Therefore, shape dependent rates of uptake are likely the reason for the increased cellular uptake of GNR-7.2 relative to GNR-4.8. Imaging of the A549 monolayer with dark-field light microscopy is not possible due to their intense background scatter. It is also worthy of note that no alteration to the biochemical homeostasis was measured in any of the cell types used following exposure to each GNR investigated (Fig. S7†), indicating that the changes in uptake can be strongly attributed to the specific physical properties of the nanomaterials and not to potential changes occurring within the cell cytoskeleton.[33]

It is also important to consider that the slight difference in ligand concentration determined by ^{1}H-NMR for the four different GNRs is only noteworthy for GNR-2.6, and cannot alone explain the presented data. The same is true for the slight zeta-potential difference between GNR-4.8 and GNR-2.6 in water, even if one was to ignore the similar zeta-potential of all samples upon incubation in supplemented cell culture medium due to the formation of a protein corona.[34] Furthermore, it could be argued that the protein corona composition is affected by the differing crystal facets of the reshaped GNRs. Given the relatively low difference in energy between the low index facets of gold, and the PVP coating, we deem this parameter to be of minimal consequence within the current experimental setting.[35]

The presence of residual CTAB on the GNRs, as determined by quantitative ^{1}H-NMR (Table S1†), is not surprising given the difficulty of removing this small ligand – a problem often highlighted by others.[22,36] However, the effective CTAB concentration in the exposure experiments is 2–7 nM corresponding to 20–50 molecules per GNR, or approximately 0.1% of a full CTAB bilayer. This is low enough so as to expect little cytotoxicity or pro-inflammatory response, as observed by the absence of any significant difference in the level of LDH, TNF-α, and IL-8 with respect to the negative control (Fig. S7†).

While a number of studies have examined the rate of cellular uptake of varying NP shapes, few have examined the shape dependence of exocytosis.[5,12,13,37] Indeed, what is being probed here is a dynamic system whereby the amount of intracellular gold is correlated with the rates of both endocytosis and exocytosis. Hypothetically, if the rate of exocytosis was inversely correlated with the aspect ratio, then higher levels of intracellular gold over time could be measured for the longer GNRs relative to the shorter ones, thereby explaining our observations. In other words, the rate limiting step regarding the quantity of intracellular gold could be exocytosis, if cellular uptake is shape-independent. To test this hypothesis, HeLa cells were incubated with GNRs for 24 h before replacing the cell culture media and subsequently measuring the quantity of exocytosed gold after 2 h, 4 h, and 6 h. HeLa cells were chosen for this experiment as they are known to readily exocytose gold NPs.[37] Assuming linearity between intracellular gold and exocytosis rates, similar quantities of gold were released from cells for all GNRs (Fig. S8†), indicating that the rate of NP exocytosis is independent of shape at the length scales investigated here and we are indeed probing only rates of shape-dependent endocytosis. Similar results were found for three different materials by Jin *et al.* whereby the exocytosis rate was

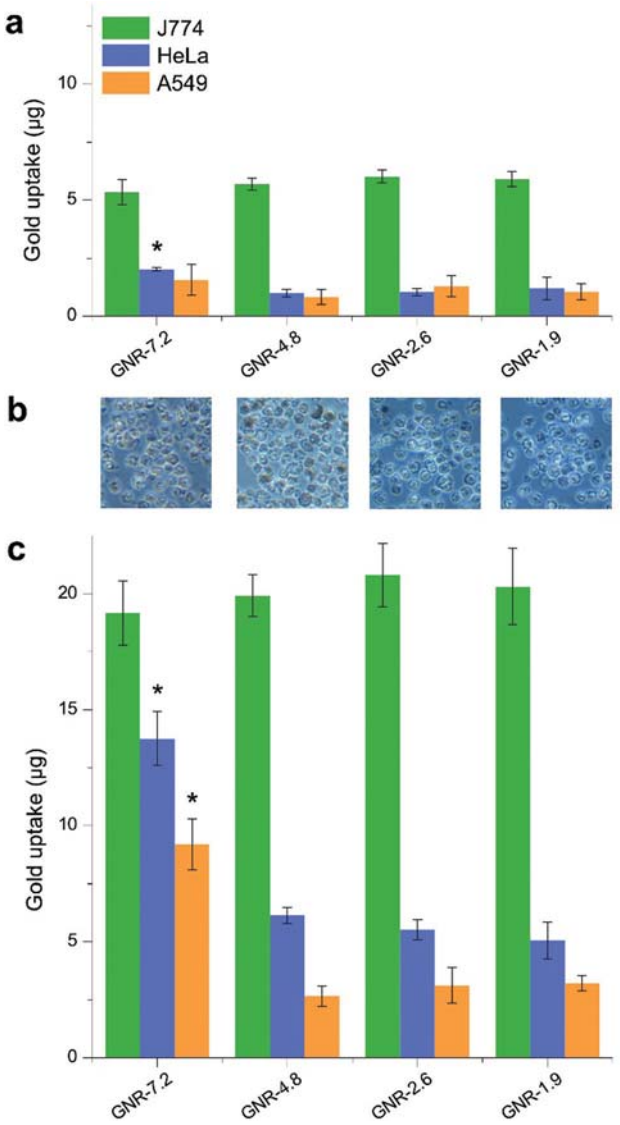

Fig. 4 Quantity of endocytosed gold nanorods. Intracellular gold measured by ICP-OES in cell lysate after iodine wash to remove extracellular GNRs. Three different cell lines were incubated with PVP coated reshaped GNRs at 40 μg mL^{-1} for either 4 h (a) or 24 h (c). (b) Phase contrast images of J774A.1 cells incubated with reshaped GNRs at 40 μg mL^{-1} for 24 h (left to right: GNR-7.2 to GNR-1.9). A two-way Tukey *post hoc* ANOVA was performed between the uptake of different aspect ratios with significant differences only found between the uptake of GNR-7.2 and all other GNRs for HeLa (4 h and 24 h time points) and A549 (24 h time point) as indicated by: *$p < 0.05$, $n = 4$.

dominated by the membrane turnover rate constant, rather than the material properties.[5]

Comparison with models

In order to explain observations of shape dependent endocytosis, the majority of published models have considered single NPs interacting with a lipid bilayer of varying receptor density, typically resulting in the identification of optimum shapes for translocation across the cellular membrane.[38–41] This could explain the increased uptake of GNR-7.2 due to its rounded cross-section that aids membrane wrapping compared to the squarer GNR-4.8 sample. However, from TEM imaging it is evident that the concept of single non-interacting NP translocation does not occur in this study (Fig. 5a–d). For all shapes and cell types used in the present study, the NPs were found as clusters both on the cell membrane and within intracellular vesicles. This finding is in agreement with a stereological study showing that gold NPs agglomerate inside the cells in (endo)lysosomes, and into larger agglomerates after prolonged times.[42] Furthermore, hyperspectral imaging of single HeLa cells, and J774A.1 cells, *via* dark-field microscopy indicated cell-associated clustering or aggregation of the nanomaterials through a blue-shift/broadening of the scattering spectra of GNR-7.2 and GNR-4.8 (insets of Fig. 5e, f and S10†).[22] While it is also possible for a red-shift to occur upon clustering, this requires clusters with a tip-to-tip geometry, which is highly unlikely in this situation. The proposed shape-dependent clustering is further supported by the absence of any shift for GNR-2.6 and GNR-1.9, along with the intense intracellular scatter of HeLa cells exposed to GNR-7.2 since individual GNRs only weakly scatter in the visible region (Fig. S11†). Given that the NPs were proven to be colloidally stable for the duration of the exposure period in supplemented cell culture medium, the clustering process can be directly associated with the presence and interaction of the GNRs with the cell membrane itself.

If clustering is taken as the rate-limiting step in cellular uptake kinetics, then it follows, logically, that the greater the residence time on the membrane the higher the probability to form NP clusters and consequently the greater the uptake.[43,44] Indeed, more GNRs were found adjacent to the membrane for the longest nanorod than any of the shorter ones. These observations are in close agreement with the predictions of Gao *et al.* who showed that the increased uptake of larger NPs, or clusters, is due to the high membrane bending energies associated with the endocytosis of smaller NPs.[45] Additionally, upon observing the angle between the membrane and the longitudinal axis of the most proximal GNRs to the membrane of the epithelial cells, *via* TEM, a propensity for the higher aspect ratio particles to bind side-on was found (Fig. S12–15†). This difference in orientation would enable the GNRs to bind to multiple receptors that trigger clustering and subsequent increased levels of cellular uptake, a concept that correlates with that reported by Grochmal *et al.*[43]

Considering clustering kinetics, a combination of experiment and simulation by Jin *et al.* could accurately model the shape dependent uptake of carbon nanotubes and other materials.[5] A key scaling metric to compare different shapes, termed the effective capture radius, was used. Crucially, the difference in the effective capture radius of the GNRs used in this study is very small, meaning that similar uptake rates would be predicted as observed for the three shorter GNRs.

The observed side-on binding of the longer GNR is evidence of a stronger overall NP-membrane adhesion force, with the probability of adhesion approximately proportional to the

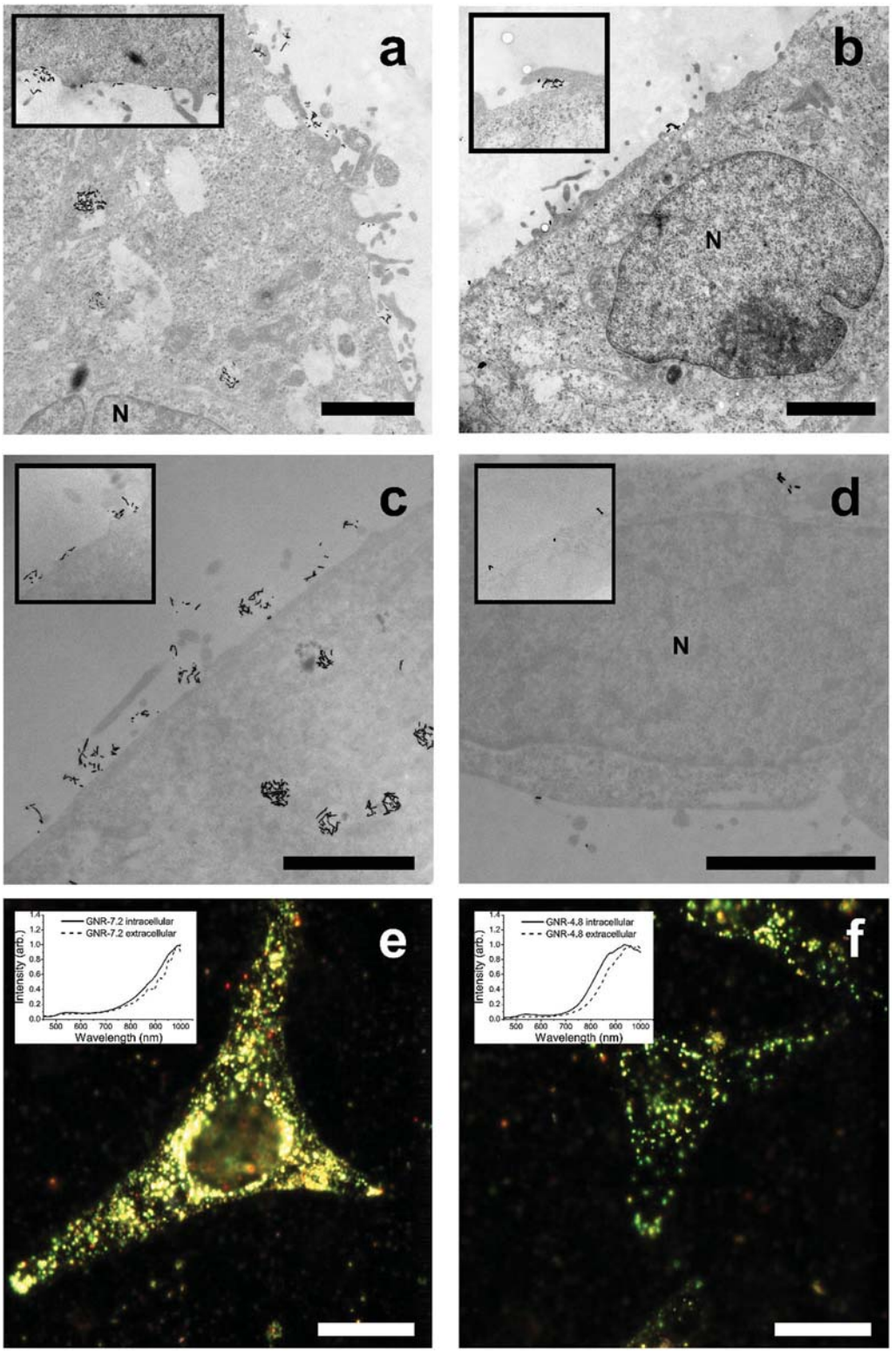

Fig. 5 Microscopy of A549 epithelial cells incubated with gold nanorods. Representative TEM micrographs of embedded, stained, and sectioned A549 and HeLa cells after incubation for 4 h with reshaped GNRs (40 μg mL^{-1}): (a) A549 with GNR-7.2, (b) A549 with GNR-4.8, (c) HeLa with GNR-7.2, and (d) HeLa with GNR-4.8. Scale bar: 2 μm. Insets: magnified micrographs of additional sections. Hyperspectral imaging combined with dark-field light microscopy of HeLa cells after incubation for 4 h with reshaped GNRs (40 μg mL^{-1}) before undergoing fixation, embedding, and imaging: (e) GNR-7.2 and (f) GNR-4.8. Scale bar, 10 μm.

contact area between particle and receptor-laden membranes.[46] Increases in this adhesion force are also predicted to increase the efficiency of endocytosis.[47] Mitragotri and co-workers have observed this shape effect for the case of polymeric particles both under flow and static conditions where rods adhere more strongly to surfaces on both synthetic and lung endothelial cell monolayers, through non-specific interactions, albeit at larger scales than the NPs used in this study.[21] Interestingly, they found that nanorods accumulated to a greater extent in the lungs and brain upon intravascular injection compared to nanospheres. These *in vivo* observations are in congruence with the increased uptake of higher aspect ratio GNRs by A549 lung epithelial cells, despite the difference in NP sizes. Indeed, Decuzzi and Ferrari predicted that above a characteristic size of 10 nm, non-spherical oblate particles in flow adhere better to membranes than spherical particles, while the trend reversed below this size regime.[46]

Our observations point to a characteristic size range around 50 nm where anisotropic and spherical NPs exhibit similar uptake kinetics. On this note, a control experiment to support this characteristic size regime through the use of spherical NPs with a similar volume to the GNRs used in this study, or indeed diameters similar to the long axis of the nanorods, could be carried out. However, to do so would require a separate, specific synthesis with subsequent functionalization steps. This would lead to NPs with different surface chemistries, as well as different particokinetics. Additionally, the NPs obtained after 6 h of thermal reshaping are near spherical themselves with an aspect ratio of 1.9. It is possible that the squared cross-section of the shorter nanorods hinders membrane wrapping and consequently their internalization. However, upon adsorption of a protein corona this geometric difference becomes negligible and therefore, combined with the lack of observation in TEM of any membrane wrapping or uptake of single GNRs, we do not consider the change in their cross-section to be of particular consequence.

Short nanorods and macrophages

The three shorter GNRs presented similar uptake efficiencies, suggestive of a characteristic dimension where anisotropy becomes important. This is supported by the experimental work of Qiu *et al.* who, despite the use of the cytotoxic and (pro-)inflammatory surfactant CTAB, found no strong shape dependence on the uptake of short GNRs.[6] Indeed, for these shorter rods the dominance of their surface chemistry eclipses any shape dependence.

The macrophages used in this study endocytosed all four samples to a similar degree indicative of different uptake mechanisms compared with the epithelial cells. Indeed, J774A.1 macrophages strongly uptake particles *via* actin-dependent macropinocytosis routes traditionally associated with larger particle uptake.[48] Additionally, the uptake of 40 nm polystyrene NPs by A549 cells can be minimized by blocking caveolin- and clathrin-mediated endocytosis.[48] The differences in size and aspect ratio of the GNR samples are small compared to the dimensions of the actin-dependent membrane ruffles involved in micropinocytosis by J774A.1 cells, explaining the lack of shape-dependent uptake of small GNRs by macrophages. Further evidence of this was provided by taking an alternative shape, nanostars, and reshaping them in DMF as for the GNRs before exposing the macrophages to three different concentrations of the reshaped, PVP-stabilised, nanostars. As expected, no shape dependent uptake was observed. Additionally, a perfect correlation between the exposed dose and the measured intracellular gold demonstrates that this study was carried out in the linear regime (Fig. S17†).

Context

To put these results into context, it is helpful to summarize complementary published research. Chithrani found a decrease in the uptake of CTAB-coated GNRs in HeLa cells as the aspect ratio increases, although Bartneck showed that these particles had poor colloidal stability in cell culture media.[13,49] Additionally, given the cytotoxicity and (pro-) inflammatory effects of CTAB it is difficult to attribute any differences in uptake to shape alone. As an example of this, another study found that 15 × 50 nm CTAB-coated GNRs were endocytosed far more efficiently than either 15 nm or 50 nm spheres.[49] Contrary to this, the uptake of transferrin coated GNRs in three different cell lines was shown to negatively correlate with aspect ratio, although the UV-Vis-NIR spectra indicated the samples were mostly nanospheres rather than rods.[12] Qiu *et al.* obtained similar results for CTAB-coated GNRs, albeit with cell viabilities of less than 50%, and upon coating with polyelectrolytes the shape effect became small – in congruence with our findings for GNR-4.8 to GNR-1.9.[6]

An elegant study by Gratton *et al.* found increased uptake of polymeric particles with their aspect ratio, albeit at a larger scale than used in this study.[8] Meng *et al.* have also shown an increase in the endocytosis rate for intermediate aspect ratios of mesoporous silica NPs – postulating HeLa and A549 cells have a shape-detecting mechanism involving Rac1 activation.[9]

Conclusions

Generalizing these findings, one could surmise that shape is not particularly important in the cellular uptake of NPs in the sub-100 nm range – a key size regime for an array of clinically relevant NPs. Previous studies have put forward contradictory views on the impact of aspect ratio and shape on NP uptake, however it is imperative to bear in mind that these materials are not molecules and, as such, other parameters such as adsorbed ligands, monodispersity, shape yields, colloidal stability, and particokinetics must be taken into account. Nevertheless, the present study highlights the lack of differentiation between cell types in terms of their uptake of small non-isotropic nanomaterials. It should be emphasized that shape can still be used in novel ways to enhance other properties of NPs such as ligand density or surface reactivity, as well as specific theranostic qualities (*e.g.* optical characteristics), while keeping in consideration that the specific

physical dimensions alone may not be the driving factor behind their observed biological impact.

Experimental

Chemicals and reagents

All chemicals were obtained from Sigma-Aldrich and used as received, unless otherwise specified. Cetyltrimethyl ammonium bromide (CTAB) and sodium oleate (NaOL) were purchased from TCI America. Hydrochloric acid (HCl, 37 wt%) was purchased from Honeywell. Deuterated methanol was purchased from Cambridge Isotope Laboratories. Ultrapure water (18 MΩ cm, Sartorius arium®) was used in all experiments. Prior to any synthesis, all glassware was rinsed with freshly prepared aqua regia followed by extensive washing with water and oven drying at 90 °C.

GNR synthesis

The GNRs were synthesized based on a modified seed-mediated co-surfactant route using CTAB and NaOL.[23] Briefly, seeds were prepared by mixing a CTAB solution (5 mL, 0.2 M) with $HAuCl_4$ (5 mL, 0.5 mM) at 30 °C and mixed gently for 5 min. A freshly prepared solution of sodium borohydride (0.6 mL of 10 mM diluted to 1 mL with water) was then rapidly added under vigorous stirring for 2 min. The seeds were used after precisely 30 min.

The growth solution was prepared by adding CTAB (7 g) and NaOL (1.234 g) to a Pyrex flask, along with water (225 mL at 50 °C) and stirred gently for 90 min to dissolve the surfactants. Over 30 min the flask was cooled to 30 °C without stirring. $AgNO_3$ (19.2 mL, 4 mM) was then added, mixed by inversion and left for 15 min. $HAuCl_4$ (200 mL, 1 mM) was added, mixed by inversion, and left untouched for 120 min. It was observed that if the solution was constantly mixed then surfactant crystals may precipitate out of solution, while the gold is sufficiently reduced without any additional mixing. Next, HCl (4.32 mL, 37 wt%) was added followed by brief inversion mixing. After 10 min, L-ascorbic acid (1 mL, 0.064 M) was introduced under vigorous stirring for 10 s. Finally, the previously prepared seeds (0.8 mL), now aged for 30 min, were added under vigorous mixing for 10 s. The GNRs were then allowed to grow overnight at 30 °C. This synthesis was repeated three times and the batches combined to make one master batch that was used in all subsequent experiments.

GNR reshaping

In order to thermally reshape the GNRs, they must be coated with polyvinylpyrrolidone (PVP, 10 kDa) and transferred to dimethylformamide (DMF). To accomplish this, the GNRs as synthesized were centrifuged (6000*g*) and redispersed to the original volume in water to reduce the bulk CTAB concentration to approximately 1 mM. PVP was then added at a concentration of 20 PVP molecules per nm^2 of GNR surface (the mean surface area was determined from TEM and a spherocylindrical model) and mixed overnight. The suspension was up-concentrated by a factor of 36 through centrifugation (6000*g*). The concentrated GNR suspension was then added dropwise under stirring to a solution of PVP in ethanol (at a concentration of 20 PVP molecules per nm^2) and mixed overnight. Once more, the GNRs were up-concentrated by a factor of 17 through centrifugation (6000*g*) with the resulting concentrated GNR suspension added dropwise under stirring to a solution of PVP in DMF (at a concentration of 20 PVP molecules per nm^2). The final ligand exchange was allowed to proceed for 4 h, before being up-concentrated by a factor of 20 through centrifugation (6000*g*). The gold concentration of the resulting PVP-GNR dispersion in DMF was 5.6 mM, and an approximate concentration of PVP was 0.05 mM.

The exchange of CTAB by PVP in ethanol is efficient, and a dense PVP shell arrests any atomic surface diffusion. We have observed this previously for the case of polyvinyl acetate/polyvinyl alcohol.[25] Therefore, a small quantity of CTAB was added to aid the process. The concentrated PVP-GNR dispersion (32 mL) was diluted in a solution of PVP in DMF (335 mL, 1 mM) and a portion of CTAB was added (13.4 mL, 27.4 mM in DMF). The dispersion was split into four separate sealed flasks (95.35 mL per flask), and the flasks were placed together in an oil bath at 140 °C and gently stirred for either 0, 90, 250, or 360 min before quenching the reaction. The four reshaped GNRs were centrifuged (8000*g*) and re-dispersed in a solution of PVP in ethanol (300 mL, 1 mM). This was repeated twice more, before a final up-concentration by centrifugation gave the stock dispersions used for later exposures. The residual concentration of DMF in the samples was predicted to be less than 0.3%, based on the remaining supernatant from each centrifugation step.

Characterization

Vis-NIR spectra were collected on a Jasco V-670 spectrophotometer. Low resolution TEM was undertaken on a Philips CM100-Biotwin microscope operating at 80 kV. Samples were prepared by drop-casting 4 μL of diluted GNRs in ethanol on a carbon-coated copper grid.

High angle annular dark field (HAADF) scanning transmission electron microscopy (STEM) images were acquired using a probe corrected Titan 60-300 microscope operated at either 200 or 300 kV. Tilt series were acquired over a tilt range of −70° to +74° using a tilt increment of 2°. A small camera length was used corresponding to an inner collection angle of 60 mrad in order to guarantee the incoherent imaging of the nanorods. Tomographic reconstructions were calculated using the simultaneous iterative reconstruction technique (SIRT). The reconstruction showing the atomic lattice was obtained using methods explained by Goris *et al.*,[26] based on high resolution projection images acquired along [100] and [110] zone axes.

Depolarized dynamic light scattering (DDLS) was carried out on a 3D LS Spectrometer (LS Instruments, Fribourg, Switzerland) equipped with a He–Ne laser (λ = 632.8 nm), as previously described.[25] Zeta-potential measurements of the reshaped GNRs were made on a Brookhaven 90Plus PALS

system. Nanoparticle tracking analysis (NTA) was carried out on a Nanosight NS500 in dilute aqueous suspensions, with identical particle detection thresholds and camera exposure times between different samples. Inductively Coupled Plasma Optical Emission Spectroscopy (ICP-OES, PerkinElmer Optima 7000 DV) was used to measure the concentration of gold in the reshaped GNR stock suspensions through dissolution of an aliquot of the stock in aqua regia.

Quantitative ^{1}H NMR spectra were collected on a Bruker 500 MHz. An aliquot of the four reshaped GNRs (0.6 mL) was transferred to deuterated methanol *via* two rounds of centrifugation. CTAB, PVP, DMF, and NaOL were also separately dissolved in deuterated methanol at known concentrations. To these eight samples, an identical amount of tetramethylsilane (TMS) was added (approximately 0.05 vol%). Therefore, after adjusting for the precise volume of sample in each NMR tube, the ratio of the integral of the TMS peak to the peak of interest with reference to this relative ratio of the pure samples gives the concentration of that particular chemical species. In addition, iodine (30 mg) was added to the GNRs over a period of four days and the samples measured once more.

Cell culture and exposure

HeLa, A549, and J774A.1 cells were cultured in a 75 cm^2 cell culture flask (Techno Plastic Products AG, Switzerland) in RPMI-1640 (Roswell Park Memorial Institute) supplemented with 10% fetal bovine serum (FBS), 100 U mL^{-1} penicillin, 100 μg mL^{-1} streptomycin, and 2 mM L-glutamine. Cells were cultured in a humidified incubator at 37 °C and 5% CO_2.

As an example of a standard uptake experiment, HeLa and J774A.1 cells were seeded 24 h prior to exposure at a density of 5×10^4 cells per well in a 24-well plate (Costar, Corning Incorporated, USA). A549 cells were seeded on PET membrane inserts with a 1 μm pore size in 12-well plates at a density of 1×10^5 cells per well and cultured for 5 days before exposure. The necessary volume of reshaped GNRs in ethanol were centrifuged and re-dispersed in water before dilution in supplemented RPMI to a working concentration of 40 μg mL^{-1} (0.2 mM), thus ensuring that the residual concentration of ethanol was less than 0.1%. After incubating the GNRs in cell culture media for 30 min, they were constantly exposed to the cells for either 4 or 24 h. The supernatant was collected for testing of any cytotoxicity or (pro-)inflammatory response. To quantify the uptake, cells were washed with PBS and a solution of I_2/KI (0.34 mM in PBS) with this washing fraction collected for gold quantification by ICP-OES. The cells were then lysed by Triton X-100 (1% in PBS) for 15 min at 37 °C with collection of the cell lysate before the addition of sodium dodecyl sulfate (SDS, 2 wt% in PBS) for 1 h and collection of this second cell lysate fraction. The two cell lysates were pooled together for analysis. In the case of the A549 exposures, the cell culture media on the basal side of the insert was also collected for analysis of GNR translocation.

Previous experiments were conducted in order to assess the suitability of the doses chosen in this study, however a different shape was used: gold nanostars. A near-identical procedure to reshaping the nanostars, as described above for the nanorods, was followed. The resulting NPs transition from highly anisotropic nanostars to near-spherical NPs. A linear dose–response was observed from 0.01–0.04 mg ml^{-1} regarding nanoparticle uptake (Fig. S17†) in J774A.1 cells, while no adverse biological effects were measured (data not shown).

Cytotoxicity and (pro-)inflammatory response

Cytotoxicity was quantified by the release of lactate dehydrogenase (LDH) into the cell culture media, an indication of damaged cell membranes, using a cytotoxicity detection kit (Roche Applied Science, Germany). Supernatants after exposure to the reshaped GNRs for 24 h were measured, with the media acting as the negative control and Triton X-100 (0.2% in PBS) as the positive control ($n = 4$).

The ability for the reshaped GNRs to induce the release of the (pro-)inflammatory cytokine TNF-α from J774A.1, or IL-8 in the case of HeLa and A549 cell-lines after 24 h suspension exposure was assessed *via* an enzyme-linked immunosorbent assay (ELISA) diagnostic kit (R&D Systems, Switzerland). Lipopolysaccharide (LPS, 100 ng mL^{-1}) in the case of J774A.1 cells, and TNF-α (50 ng mL^{-1}) in the case of HeLa and A549 cells, acted as the positive control at a concentration of 1 μg mL^{-1} ($n = 4$).

Interference

Potential interference through cytokine adsorption to the GNRs was previously observed to be negligible.

Spectrometric interference from the LSPR absorbance bands was minimized for the cytotoxicity assay through measurement of the rate of change of the absorption at 490 nm, within the linear dynamic range, as opposed to measurement of the absorbance at a single time-point.

Quantification of uptake

The amount of gold in the three fractions (supernatant, iodine wash, and cell lysate) from the suspension exposures was quantified *via* ICP-OES. Briefly, an aliquot of the collected fraction was added to a solution of Triton X-100 (1 mL, 2%) along with HNO_3 (0.4 mL, 67 wt%), and heated to 70 °C for 2 h. Finally, HCl (1.6 mL, 37 wt%) was added and made up to 5 mL with water and analyzed on a PerkinElmer Optima 7000 DV ICP-OES.

Preparation of cells for microscopy

Electron microscopy. Cells were cultured on membrane inserts at the same density as described above before constant exposure for 4 h to reshaped GNRs at the same concentrations as stated for the uptake experiments. The cells were then washed and fixed in glutaraldehyde, post-fixed with osmium tetroxide, dehydrated in increasing concentrations of ethanol, before embedding in Epon resin. Ultrathin sections (70 nm) were cut on a Reichert-Jung Ultracut E microtome and placed on single-slot copper grids, and then stained with uranyl acetate and lead citrate. The samples were imaged on a Philips CM100-Biotwin microscope operating at 80 kV.

Dark-field microscopy. HeLa and J774A.1 cells were cultured as described above except that sterile round coverslips were used within wells. After 4 h or 24 h constant exposure to the reshaped GNRs the cells were washed 3× with PBS, fixed with 1% paraformaldehyde for 15 min at room temperature prior to being stained with rhodamine phalloidin (132 nM) and 4′,6-diamidino-2-phenylindole (DAPI, 3.6 μM) for 120 min at room temperature in the dark. Samples were then embedded upon microscope slides using Glycergel® (Dako). Imaging was undertaken on a dark-field light microscopy system from CytoViva equipped with a hyperspectral camera and data was analyzed using ENVI software (Exelis Visual Information Systems). Hyperspectral images were recorded with a 100× oil immersion lens at three different focal planes: on the background glass slide, in the middle of the cell, and on the top of the cell to ensure only internalized GNRs were analyzed. The mean spectra of individual GNRs attached to the underlying glass coverslip gives the spectra for extracellular particles enabling compensation for differences in the refractive index of the embedding medium. The recorded spectra were normalized to recently recorded lamp spectra before being smoothed by a Savitzky–Golay filter.

Author contributions

C. K., L. R. L. and M. J. D. C. developed the concept and planned the experiments. C. K. performed the experiments and data analysis, with B. G. and S. B. undertaking the 3D investigation of the GNRs. B. R. R. and A. P. F. supervised the work. C. K. wrote and all authors edited the manuscript. All authors have given approval to the final version of the manuscript.

Acknowledgements

The authors would like to thank C. Endes for her help and technical assistance with all cell culture experiments. The work was supported by the Adolphe Merkle Foundation, the Swiss National Science Foundation (PP00P2_123373), the Swiss National Science Foundation through the National Centre of Competence in Research Bio-Inspired Materials, the Flemish Fund for Scientific Research (FWO Vlaanderen) through a postdoctoral research grant, and the European Research Council (ERC Starting Grant #335078-COLOURATOMS). The authors also appreciate financial support from the European Union under the Seventh Framework Program (Integrated Infrastructure Initiative N. 262348 European Soft Matter Infrastructure, ESMI).

Notes and references

1 P. Rivera-Gil, D. Jimenez de Aberasturi, V. Wulf, B. Pelaz, P. del Pino, Y. Zhao, J. M. de la Fuente, I. Ruiz de Larramendi, T. Rojo, X. J. Liang and W. J. Parak, *Acc. Chem. Res.*, 2013, **46**, 743–749.
2 N. P. Truong, M. R. Whittaker, C. W. Mak and T. P. Davis, *Expert Opin. Drug Delivery*, 2015, **12**, 129–142.
3 D. B. Chithrani, *Mol. Membr. Biol.*, 2010, **27**, 299–311.
4 L. Florez, C. Herrmann, J. M. Cramer, C. P. Hauser, K. Koynov, K. Landfester, D. Crespy and V. Mailander, *Small*, 2012, **8**, 2222–2230.
5 H. Jin, D. A. Heller, R. Sharma and M. S. Strano, *ACS Nano*, 2009, **3**, 149–158.
6 Y. Qiu, Y. Liu, L. Wang, L. Xu, R. Bai, Y. Ji, X. Wu, Y. Zhao, Y. Li and C. Chen, *Biomaterials*, 2010, **31**, 7606–7619.
7 J. Wang, J. D. Byrne, M. E. Napier and J. M. DeSimone, *Small*, 2011, **7**, 1919–1931.
8 S. E. Gratton, P. A. Ropp, P. D. Pohlhaus, J. C. Luft, V. J. Madden, M. E. Napier and J. M. DeSimone, *Proc. Natl. Acad. Sci. U. S. A.*, 2008, **105**, 11613–11618.
9 H. Meng, S. Yang, Z. Li, T. Xia, J. Chen, Z. Ji, H. Zhang, X. Wang, S. Lin, C. Huang, Z. H. Zhou, J. I. Zink and A. E. Nel, *ACS Nano*, 2011, **5**, 4434–4447.
10 K. Donaldson, F. A. Murphy, R. Duffin and C. A. Poland, *Part. Fibre Toxicol.*, 2010, **7**, 5.
11 C. A. Poland, R. Duffin, I. Kinloch, A. Maynard, W. A. Wallace, A. Seaton, V. Stone, S. Brown, W. Macnee and K. Donaldson, *Nat. Nanotechnol.*, 2008, **3**, 423–428.
12 B. D. Chithrani and W. C. Chan, *Nano Lett.*, 2007, **7**, 1542–1550.
13 B. D. Chithrani, A. A. Ghazani and W. C. Chan, *Nano Lett.*, 2006, **6**, 662–668.
14 A. M. Alkilany and C. J. Murphy, *J. Nanopart. Res.*, 2010, **12**, 2313–2333.
15 V. Hirsch, C. Kinnear, L. Rodriguez-Lorenzo, C. A. Monnier, B. Rothen-Rutishauser, S. Balog and A. Petri-Fink, *Nanoscale*, 2014, **6**, 7325–7331.
16 J. G. Teeguarden, P. M. Hinderliter, G. Orr, B. D. Thrall and J. G. Pounds, *Toxicol. Sci.*, 2007, **95**, 300–312.
17 V. Hirsch, C. Kinnear, M. Moniatte, B. Rothen-Rutishauser, M. J. Clift and A. Fink, *Nanoscale*, 2013, **5**, 3723–3732.
18 B. Parakhonskiy, M. V. Zyuzin, A. Yashchenok, S. Carregal-Romero, J. Rejman, H. Mohwald, W. J. Parak and A. G. Skirtach, *J. Nanobiotechnol.*, 2015, **13**, 53.
19 K. D. Young, *Curr. Opin. Microbiol.*, 2007, **10**, 596–600.
20 E. M. Grzincic and C. J. Murphy, *ACS Nano*, 2015, **9**, 6801–6816.
21 P. Kolhar, A. C. Anselmo, V. Gupta, K. Pant, B. Prabhakarpandian, E. Ruoslahti and S. Mitragotri, *Proc. Natl. Acad. Sci. U. S. A.*, 2013, **110**, 10753–10758.
22 C. Kinnear, H. Dietsch, M. J. Clift, C. Endes, B. Rothen-Rutishauser and A. Petri-Fink, *Angew. Chem., Int. Ed.*, 2013, **52**, 1934–1938.
23 X. Ye, C. Zheng, J. Chen, Y. Gao and C. B. Murray, *Nano Lett.*, 2013, **13**, 765–771.
24 L. Rodriguez-Lorenzo, J. M. Romo-Herrera, J. Perez-Juste, R. A. Alvarez-Puebla and L. M. Liz-Marzan, *J. Mater. Chem.*, 2011, **21**, 11544–11549.

25 C. Kinnear, D. Burnand, M. J. Clift, A. F. Kilbinger, B. Rothen-Rutishauser and A. Petri-Fink, *Angew. Chem., Int. Ed.*, 2014, **53**, 12613–12617.

26 B. Goris, S. Bals, W. Van den Broek, E. Carbo-Argibay, S. Gomez-Grana, L. M. Liz-Marzan and G. Van Tendeloo, *Nat. Mater.*, 2012, **11**, 930–935.

27 E. Carbo-Argibay, B. Rodriguez-Gonzalez, J. Pacifico, I. Pastoriza-Santos, J. Perez-Juste and L. M. Liz-Marzan, *Angew. Chem., Int. Ed.*, 2007, **46**, 8983–8987.

28 E. Carbo-Argibay, B. Rodriguez-Gonzalez, I. Pastoriza-Santos, J. Perez-Juste and L. M. Liz-Marzan, *Nanoscale*, 2010, **2**, 2377–2383.

29 A. E. Nel, L. Madler, D. Velegol, T. Xia, E. M. Hoek, P. Somasundaran, F. Klaessig, V. Castranova and M. Thompson, *Nat. Mater.*, 2009, **8**, 543–557.

30 E. C. Cho, J. Xie, P. A. Wurm and Y. Xia, *Nano Lett.*, 2009, **9**, 1080–1084.

31 D. Vanhecke, L. Rodriguez-Lorenzo, M. J. D. Clift, F. Blank, A. Petri-Fink and B. Rothen-Rutishauser, *Nanomedicine*, 2014, **9**, 1885–1900.

32 C. Rosman, S. Pierrat, A. Henkel, M. Tarantola, D. Schneider, E. Sunnick, A. Janshoff and C. Sonnichsen, *Small*, 2012, **8**, 3683–3690.

33 A. Panariti, G. Miserocchi and I. Rivolta, *Nanotechnol., Sci. Appl.*, 2012, **5**, 87–100.

34 S. Tenzer, D. Docter, J. Kuharev, A. Musyanovych, V. Fetz, R. Hecht, F. Schlenk, D. Fischer, K. Kiouptsi, C. Reinhardt, K. Landfester, H. Schild, M. Maskos, S. K. Knauer and R. H. Stauber, *Nat. Nanotechnol.*, 2013, **8**, 772–781.

35 Q. Jiang, H. M. Lu and M. Zhao, *J. Phys.: Condens. Matter.*, 2004, **16**, 521–530.

36 L. Vigderman, P. Manna and E. R. Zubarev, *Angew. Chem., Int. Ed.*, 2012, **51**, 636–641.

37 R. Sakhtianchi, R. F. Minchin, K. B. Lee, A. M. Alkilany, V. Serpooshan and M. Mahmoudi, *Adv. Colloid Interface Sci.*, 2013, **201–202**, 18–29.

38 P. Decuzzi and M. Ferrari, *Biophys. J.*, 2008, **94**, 3790–3797.

39 Y. Li, T. Yue, K. Yang and X. Zhang, *Biomaterials*, 2012, **33**, 4965–4973.

40 S. Nangia and R. Sureshkumar, *Langmuir*, 2012, **28**, 17666–17671.

41 R. Vacha, F. J. Martinez-Veracoechea and D. Frenkel, *Nano Lett.*, 2011, **11**, 5391–5395.

42 C. Brandenberger, C. Muhlfeld, Z. Ali, A. G. Lenz, O. Schmid, W. J. Parak, P. Gehr and B. Rothen-Rutishauser, *Small*, 2010, **6**, 1669–1678.

43 A. Grochmal, E. Ferrero, L. Milanesi and S. Tomas, *J. Am. Chem. Soc.*, 2013, **135**, 10172–10177.

44 A. Saric and A. Cacciuto, *Soft Matter*, 2013, **9**, 6677–6695.

45 H. Gao, W. Shi and L. B. Freund, *Proc. Natl. Acad. Sci. U. S. A.*, 2005, **102**, 9469–9474.

46 P. Decuzzi and M. Ferrari, *Biomaterials*, 2006, **27**, 5307–5314.

47 P. Decuzzi and M. Ferrari, *Biomaterials*, 2007, **28**, 2915–2922.

48 D. A. Kuhn, D. Vanhecke, B. Michen, F. Blank, P. Gehr, A. Petri-Fink and B. Rothen-Rutishauser, *Beilstein J. Nanotechnol.*, 2014, **5**, 1625–1636.

49 M. Bartneck, H. A. Keul, S. Singh, K. Czaja, J. Bornemann, M. Bockstaller, M. Moeller, G. Zwadlo-Klarwasser and J. Groll, *ACS Nano*, 2010, **4**, 3073–3086.